15TH IEA HEAT PUMP CONFERENCE
MAY 26–29, 2026 | HOFBURG
VIENNA 2026
DECARBONISATION THROUGH INNOVATION

# Performance enhancement of a steam generation heat pump with multi-stage compression and an internal heat exchanger under large temperature lift

Hongryul Joo[a], Min Soo Kim[a]

[a]*Department of Mechanical Engineering, Seoul National University, 1 Gwanak-ro, Gwanak-gu, Seoul 08826, Republic of Korea*

**Abstract**

Steam generation heat pump (SGHP) has emerged as a key technology for the electrification of heat and the reduction of carbon emissions. Many studies have focused on increasing steam generation temperature using mechanical vapor recompression (MVR) systems, which utilize waste heat at temperatures above 60°C. As industrial processes become more segmented and energy efficiency improves, the temperature of available waste heat for SGHP applications tends to be limited. To broaden the application of SGHP, their performance under low-grade waste heat needs to be enhanced. In this study, a multi-stage compression system with vapor injection and an internal heat exchanger was adopted to improve the performance of SGHP under a large temperature lift of more than 100°C. The proposed system is capable of generating up to 140°C steam from a 20°C heat source using R1233zd(E) refrigerant. Simulation results confirmed enhanced performance across a broad range of source temperatures, with particularly notable improvements at large temperature lift. The system achieved second-law efficiency exceeding 60%, which is higher than the performance reported in previous studies. This will provide a basis for evaluating the energy consumption, carbon reduction potential, and economic feasibility of SGHP compared to fossil fuel boilers across a wide range of heat source temperatures.



*Keywords: Steam genreation heat pump; Large temperature lift; Low-temperature waste heat; Internal heat exchanger*

## 1. Introduction

Energy consumption in the industrial sector accounts for about 30% of total global energy use. Among this approximately 75% of industrial energy is utilized as thermal energy for processes with a wide temperature range from low temperature heat below 150°C to over 400°C [1-2]. According to net zero by 2050 scenario proposed by the International Energy Agency (IEA), the IEA emphasizes the need to increase the adoption of heat pumps and plans to ban the sale of new fossil fuel boilers by 2025 [3]. High temperature heat pump (HTHP) or steam generation heat pump (SGHP) are getting attention as promising alternatives of conventional industrial boilers below 200°C, as they can significantly reduce carbon emissions and contribute to carbon neutrality. When powered by renewable electricity, SGHP can enable carbon-free steam generation.

The heating temperature of a heat pump is limited by the characteristic of refrigerant, particularly its critical temperature. Most refrigerants used in commercial heat pumps for space heating have critical temperature below 100°C. Many studies have been conducted to find suitable refrigerants for SGHP with higher critical temperatures above 100°C, while also complying with increasingly strict refrigerant regulations on global warming potential (GWP), such as those established by the Kigali Amendment. Many studies have compared various refrigerants for SGHP in terms of both environmental impact and performance such as R600, R1336mzz(Z), R1233zd(E), R245fa, and R1234ze(E) [4-8]. Among these, R1233zd(E) and R600 have shown highest potential for SGHP application compared to other refrigerants [9]. Recently, R1233zd(E) has been widely adopted in studies on SGHP applications due to its high critical temperature (166.5°C), safe operating characteristics, and low GWP (GWP=1) [10-12].

Extensive research has been conducted to enhance the heating capacity and efficiency of SGHP [13-16]. Appragus et al. experimentally investigated the performance improvement achieved by incorporating an internal heat exchanger in a single-stage cycle using R1224yd(Z), R1233zd(E), R1336mzz(Z), and R245fa as refrigerants, and tested steam generation temperature up to 150°C [17-18]. Kang et al. conducted experiments to investigate the effect of an internal heat exchanger using R245fa, and found that its incorporation increased both the steam generation rate and the system coefficient of performance (COP) in a single-stage cycle [19]. Wu et al. developed a SGHP system employing economized vapor injection with R1233zd(E), achieving a condensing temperature up to 145°C and exhibiting superior efficiency compared to other refrigerants [20].

However, most studies have focused on SGHP system utilizing medium or high-grade waste heat source above 60°C. With the increasing efficiency of industrial processes for energy saving and the growing utilization of waste heat, it has become more difficult to use medium-grade waste heat. Therefore, recent research has been conducted employing low-grade waste heat, which involves a large temperature lift between the heat source outlet and the heat sink inlet [21-24]. Dong et al. developed a cascade HTHP system using HP-1 as the refrigerant in the high-temperature cycle (HTC) and R1234ze(E) in the low-temperature cycle (LTC) to improve system performance under low temperature heat source conditions, achieving maximum COP of 2.20 at a heat source temperature of 20°C with a temperature lift of 100 K by optimizing the intermediate temperature and the vapor injection pressure [25]. Ma et al. constructed an air-source SGHP with an autocascade cycle to recover low temperature air sources, resulting in a COP of 1.42 at an air source temperature of -30°C and generating 170°C steam through water vapor compression [26-27].

Although these studies have been investigated SGHP systems with large temperature lifts above 100 K utilizing low-grade waste heat, most of them have focused on cascade cycle configurations and have not sufficiently investigated alternative cycle design for improving efficiency, such as multi-stage compression (three-stages or more) and the integration of internal heat exchangers within multi-stage cycles. In this study, a three-stage compression cycle incorporating an internal heat exchanger was proposed to enhance the efficiency of a large temperature difference SGHP utilizing low-grade waste heat source. A simulation model for SGHP was developed to analyze the system performance, which can generate steam up to 140°C with varying heat source temperatures ranging from 20°C to 80°C. The system performance and system efficiency were compared across several cycle configurations and against results from previous studies.

## 2. Model development

### *2.1. Refrigerant selection*

R600, R601, R1233zd(E), and R1336mzz(Z) have been identified as suitable refrigerants for SGHP due to their high critical temperatures and thermodynamic performance [9-12]. Fig. 1 shows the thermodynamic properties of potential refrigerants for SGHP application, calculated using REFPROP 10.0 [28]. Although R600 and R601 exhibit large latent heat and high critical temperatures, high flammability limits their practical application in SGHP systems. R1233zd(E) has thermodynamic properties similar to those of R245fa, which has been widely used as a high-temperature heat pump refrigerant but is being replaced due to its high GWP (GWP=1030) [2,13,19]. Considering its favorable characteristics, such as of very low GWP, high critical temperature, large latent heat, and non-toxicity, R1233zd(E) was selected as the refrigerant of the simulated SGHP system.

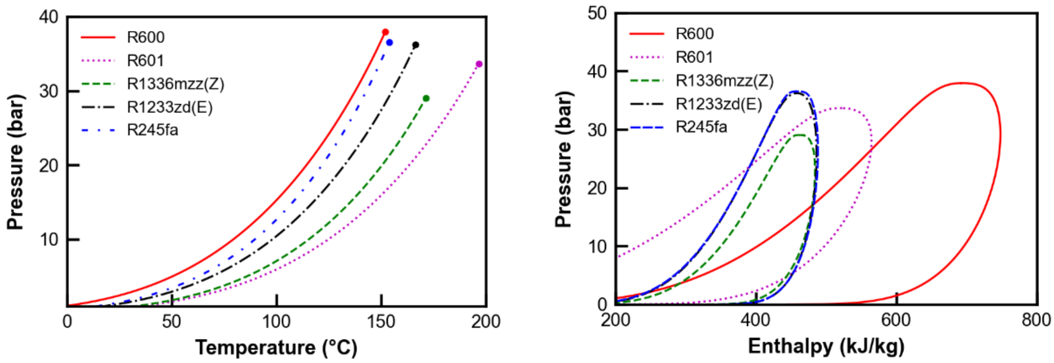


(a) (b)

Fig. 1. Thermodynamic characteristics of SGHP refrigerants: (a) P-T diagram, and (b) P-h diagram

### *2.2. Component modeling*

The thermodynamic properties of R1233zd(E) and water were calculated using NIST REFPROP 10.0 [28]. Each component in SGHP system was modeled under steady-state conditions with Python-based code. The heat transfer coefficient correlations for evaporation and condensation of R1233zd(E) in the plate heat exchanger were adopted from the experimental studies of Lee et al. and Kwon et al. [29-30]. Heat transfer and pressure drop in the plate heat exchangers were calculated for each segmented element using the finite volume method (FVM). The governing equations for each segmented element heat transfer are presented in Eq. (1)-(3).

For a steady-state reciprocating compressor model, the refrigerant mass flow rate is calculated as the product of the inlet density, compressor rotational speed, displacement volume, and volumetric efficiency. The compressor outlet enthalpy and temperature are then determined based on the pressure ratio and compressor efficiency. The polytropic efficiency of the compressor was assumed to be 0.75, based on previous studies on reciprocating compressor model [6, 26]. The expansion valve was modelled as an isenthalpic throttling process, in which the refrigerant expands without any heat exchange or work input. The mass flow rate through the expansion valve was calculated using the orifice flow equation in Eq. (4).

$$Q = \varepsilon C_{min}(T_{h,in} - T_{c,in}) \tag{1}$$

$$\varepsilon = f(\frac{UA}{C_{min}}, \frac{C_{min}}{C_{max}}) \tag{2}$$

$$UA = \frac{1}{\frac{1}{\alpha_h A_s} + \frac{1}{\alpha_c A_s} + \frac{L}{k A_s} + R_f^{"}} \tag{3}$$

$$\dot{V} = K_v \sqrt{\left(\frac{\rho_w}{\rho}\right) \Delta P} \tag{4}$$

### *2.3. Cycle configurations*

#### *2.3.1. Multi-stage compression*

In heat pump cycle, a multi-compression system with vapor injection is employed to enhance compressor efficiency by reducing the pressure ratio across the condensation and evaporation processes. In addition, vapor injection decreases the degree of superheat (DSH) at compressor inlet, which can further improve compressor performance, as described in Eq. (5). These effects become more significant under higher compression ratios and larger temperature differences between the evaporator and the condenser.

$$\dot{W}_{comp} = \dot{m}(h_{out} - h_{in}) \approx \dot{m}\frac{\gamma}{\gamma-1} R T_{in}\left[\left(\frac{P_{out}}{P_{in}}\right)^{\frac{\gamma-1}{\gamma}} - 1\right] \tag{5}$$

$$\eta_{II} = \frac{COP_{actual}}{COP_{Carnot}} \tag{6}$$

Fig. 2 shows the COP and second-law efficiency, as described by Eq. (6), obtained from the simulation of a multi-compression cycle as a function of temperature lift for the target SGHP system designed to generate 120°C steam from 20°C water heat source, corresponding to a temperature lift of over 100 K. The COP and second-law efficiency increase meaningfully up to three-stage compression across the entire temperature difference range, while further improvement becomes noticeably smaller from four-stages.

As shown in Table 1, For a source inlet temperature of 20°C, the two-stage compression cycle increase the COP by approximately 34.1%, representing the most significant improvement. The three-stage compression cycle provides an additional 8.0% increase in COP compared with the two-stage compression, while the four-stage compression cycle shows only a marginal improvement. It can be seen that the three-stage compression represent the most suitable configuration for an SGHP system operating with a temperature lift exceeding 100 K, and this effect becomes more pronounced at large temperature lifts. When compared with a cascade cycle using R1233zd(E) in the top cycle with two-stage compression and R1234ze(E) in the bottom cycle with a single-stage, the three-stage compression system indicates higher efficiency. This is primarily because R1233zd(E) has favourable characteristics comparable to those other working fluids used in the bottom cycle.

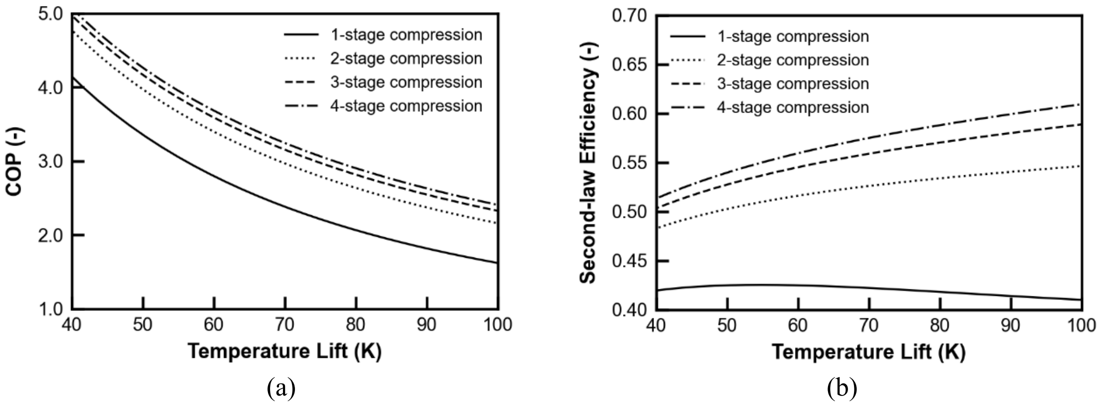


Fig. 2. Simulation results for multi-compression cycle (a) COP change, (b) second-law efficiency ($T_{source,in}$=20°C, $T_{sink,in}$=120°C)

Moreover, the multi-stage compression cycle reduces the refrigerant mass flow rate in the bottom stage, thereby decreasing the required volumetric flow rate of the compressor at low temperature, where the refrigerant density is low. Among the various vapor injection configurations between compression stages, the flash-tank vapor injection type calculated the best performance and allows for easier control of the intermediate pressure for the target SGHP system. The optimal intermediate pressure was determined through iterative calculations using the python SciPy optimization library.

Table 1. Simulation results for serval cycle configurations ($T_{source,in}$=20°C, $T_{sink,in}$=120°C)

| Parameter | 1-stage compression | 2-stage compression | 3-stage compression | Cascade cycle |
|---|---|---|---|---|
| Refrigerant | R1233zd(E) | R1233zd(E) | R1233zd(E) | R1234ze(E) / R1233zd(E) |
| COP [-] | 1.58 | 2.12 | 2.29 | 2.20 |
| COP improvement | - | 34.1% | 8.0% | |
| 2nd law efficiency [-] | 0.41 | 0.55 | 0.59 | 0.57 |

*2.3.2. Internal heat exchanger*

The internal heat exchanger is a component that transfers heat between the liquid refrigerant leaving the condenser and the vapor refrigerant leaving the evaporator. A higher DSH and degree of subcooling (DSC) improves system stability and increases heating capacity by raising the compressor inlet and outlet temperatures. While the compressor work remains nearly constant with only a slight increase, the adoption of internal heat exchanger enhances both the heating capacity and the COP, as reported in [17-19]. However, in a multi-stage compression system, there are several possible configurations for integrating an internal heat exchanger, depending on the connection location within the refrigerant circuit. When the internal heat exchanger is connected between the evaporator outlet and the high temperature liquid refrigerant line in a three-stage compression cycle, three configuration options can be considered: (1) connection to the condenser outlet, (2) connection to the second stage expansion valve inlet, and (3) connection to the first stage expansion valve inlet.

Fig. 3 shows the simulation results for three configurations integrating an internal heat exchanger, evaluated under the same pressure ratio for each compression stage. According to the simulation results, configuration (c), in which the internal heat exchanger was connected to the first stage expansion valve, showed the highest COP of 2.32, followed by configuration (b) connected to the second stage expansion valve with a COP of 2.27. Configuration (a), with the internal heat exchanger connected to the condenser outlet, exhibited the lowest COP of 2.22, which was even lower than that of the system without an internal heat exchanger.

Although several thermodynamic effects influence the cycle performance, the main factor is the inherent characteristic of the multi-compression cycle with vapor injection, in which the refrigerant mass flow rate becomes smaller in the lower stage. When the internal heat exchanger is connected to the higher stage liquid refrigerant line, the enthalpy of the refrigerant entering the expansion valve decreases, reducing the vapor injection mass flow rate. As a result, the lower stage refrigerant flow is not decreased as effectively, and the cooling effect of injection process is weakened.

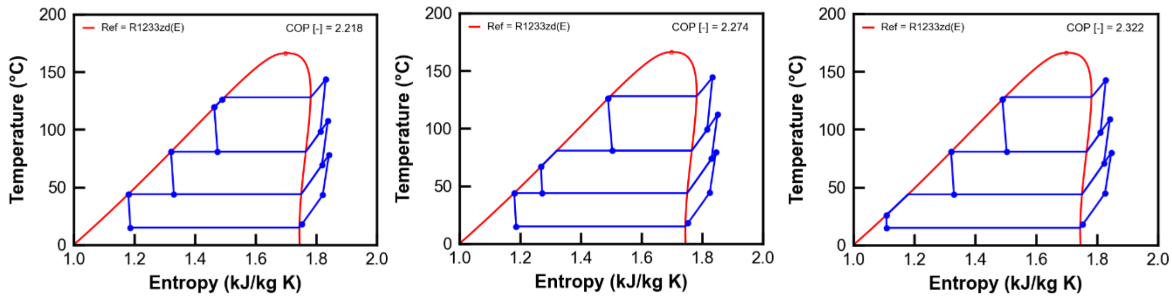

(a) (b) (c)

Fig. 3. Simulation results for SGHP configurations with an internal heat exchanger: (a) condenser outlet, (b) second stage expansion valve inlet, (c) first stage expansion valve inlet.

Consequently, incorporating an internal heat exchanger increases the heating capacity by raising the compressor discharge temperature. However, connecting it to an upper stage increases the compressor power consumption due to the elevated mass flow rate in the lower stage. Therefore, coupling the internal heat exchanger to the first stage expansion valve inlet provides the greatest improvement in COP while having minimal impact on the injection mass flow rate.

Nevertheless, the resulting rise in compressor inlet and outlet temperatures may impose thermal limitations due to lubrication and circuit cooling [17-18]. In this study, the maximum compressor discharge temperature was limited to 150°C by controlling effectiveness of the internal heat exchanger, as shown in Eq. (1).

### *2.4. System configuration*

In this study, SGHP system was constructed with three-stage compressors, a condenser, an evaporator, an internal heat exchanger, including steam generation part, as shown in Fig. 4. The refrigerant evaporates by absorbing heat from the low-temperature water heat source, is compressed through three-stage compressors, and transfers heat to the water in the condenser. It is then separated into saturated vapor and liquid in the flash tank; the vapor is directed to the intermediate stage of the compressor, while the liquid flows to the expansion valve. For the steam generation system, water is pumped to the condenser, where it is pressurized and heated, and then expanded before entering the steam tank. The feedwater temperature was assumed to be equal to the steam generation temperature. Accordingly, the heating capacity of SGHP was converted into the latent heat required for steam evaporation in the steam generator. Detailed system configurations used in simulation models and planned for future experimental implementation are shown in Table 2.

Table 2. Component configurations of SGHP system

| Component | Model | Description |
|---|---|---|
| Refrigerant | - | R1233zd(E) |
| 1st stage compressor | Dorin H392CS | $\dot{v}_{dis}$=27.97 m$^3$/h (60 Hz), Polytropic efficiency=0.75 |
| 2nd stage compressor | Dorin H151CS | $\dot{v}_{dis}$=9.00 m$^3$/h (60 Hz), Polytropic efficiency=0.75 |
| 3rd stage compressor | Dorin H101CC | $\dot{v}_{dis}$=6.44 m$^3$/h (60 Hz), Polytropic efficiency=0.75 |
| Evaporator | DIC-503- | L=503 mm, W=123 mm, $N_P$=21 |
| Condenser | JUH-503 | L=503 mm, W=123 mm, $N_P$=35 |
| Internal heat exchanger | DIC-285 | L=285 mm, W=230 mm, $N_P$=17 |

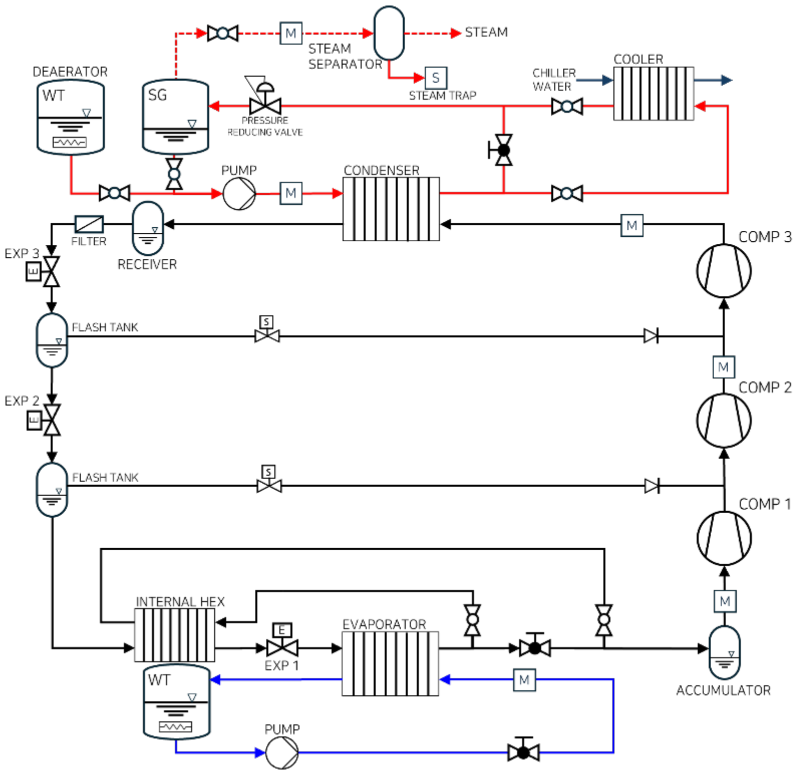


Fig. 4. Schematic diagram of the simulated SGHP system

Because of the low density of R1233zd(E) refrigerant near its normal boiling point (NBP = 18°C), 1st stage compressor require a large displacement volume to meet the designed mass flow rate. The geometries of the heat exchangers (condenser and evaporator) were determined based on the target DSH, DSC, and approach temperature, which represents the temperature difference between the saturation temperature and the water outlet temperature. In the proposed SGHP system, the DSH and approach temperature of the evaporator were set to 3 K and 3.7 K, respectively, while the DSC and approach temperature of the condenser were set to 3 K and 5.7 K under the target operating condition designed to generate 120°C steam from a 20°C water heat source.

*2.5. Simulation conditions*

The simulation conditions used in this study are summarized in Table 3. The heating capacity of the SGHP was set to 10 kW. The heat source inlet temperature was varied from 20°C to 80°C, and the heat sink temperature (steam generation temperature) was controlled between 120°C and 140°C, which are below the critical temperature of the R1233zd(E) refrigerant (166.5°C). The water mass flow rates of the heat source and heat sink were each varied from 0.5 to 1.5 kg/s. The performance of internal heat exchanger was controlled by adjusting its effectiveness from 0 to 0.6, achieved by regulating the mass flow rate of the evaporator outlet stream entering the heat exchanger. The compressor speed and expansion valve opening were regulated based on the designed refrigerant mass flow rate at each stage.

**3. Simulation results**

Fig. 5 shows the steady-state simulation results of the proposed three-stage compression system incorporating an internal heat exchanger in the first stage. The maximum system COP was calculated to be 2.39 under the target operating condition, generating 120°C steam from a 20°C water heat source, corresponding to a temperature lift exceeding 100 K. Fig. 6 presents the variations in COP and compressor discharge temperature with varying internal heat exchanger effectiveness values. As the effectiveness of the internal heat exchanger increased, the system COP also improved; however, the compressor discharge temperature exceeded the temperature limit of 150°C. The maximum allowable effectiveness of the internal heat exchanger was 0.44 for a steam generation temperature of 120°C, 0.22 for 130°C, and 0 for 140°C as the compressor discharge temperature exceeded the limit of 150°C at higher effectiveness values.

Table 3. SGHP simulation conditions

| Parameter | Value |
|---|---|
| Heating capacity | 10 [kW] |
| Heat source inlet temperature | 20 – 80 [℃] |
| Heat source water mass flow rate | 0.5 – 1.5 [kg/s] |
| Heat sink inlet temperature | 120 – 140 [℃] |
| Heat sink water mass flow rate | 0.5 – 1.5 [kg/s] |
| Effectiveness of internal heat exchanger | 0 – 0.6 [-] |

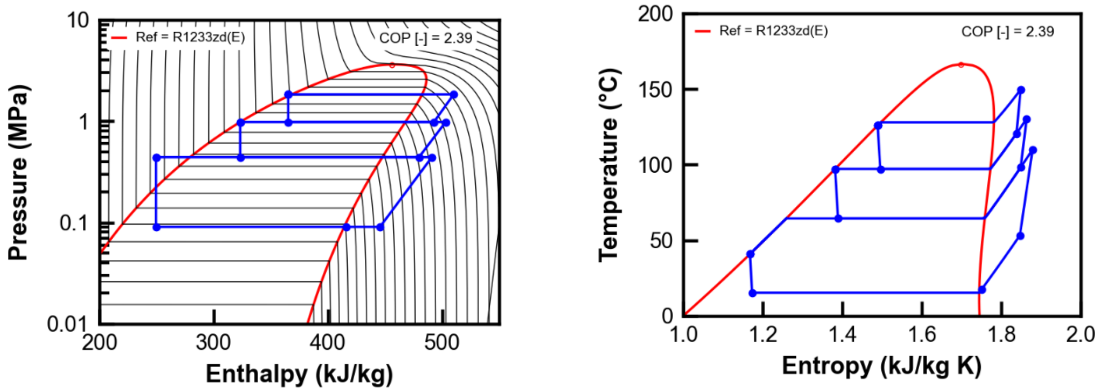


Fig. 5. Simulation results for the SGHP system: (a) P–h diagram, (b) T–s diagram.

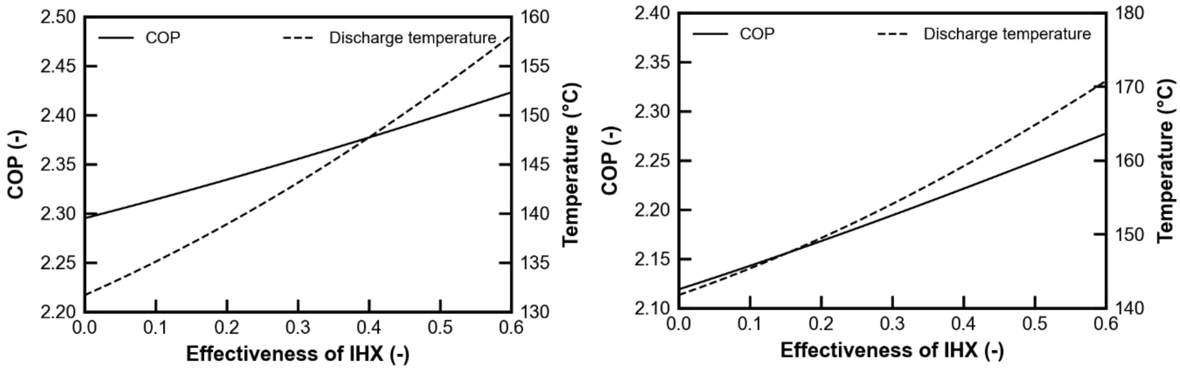


Fig. 6. Variation of COP with the effectiveness of the internal heat exchanger: (a) steam temperature of 120°C, (b) steam temperature of 140°C

Fig. 7 (a) shows the system maximum COP as a function of the water heat source inlet temperature ranging from 20°C to 80°C. For a steam generation temperature of 120°C, the system maximum COP was calculated to be 2.75 at a heat source inlet temperature of 40°C and 3.63 at 60°C, corresponding to a maximum increase of 4.6% with the adoption of the internal heat exchanger. For a higher steam generation temperature of 130°C, the COP decreased, with values of 1.96 at a heat source inlet temperature of 20°C and 2.28 at 40°C. Fig. 7 (b) illustrates the total system COP when the SGHP is combined with a mechanical vapor recompression (MVR) system to further increase the steam temperature. With an MVR compressor isentropic efficiency of 0.7, the total COP was calculated as 2.00 for a final steam temperature of 160°C and 1.78 for 200°C, based on the SGHP steam generation temperature of 120°C with the heat source temperature of 20°C.

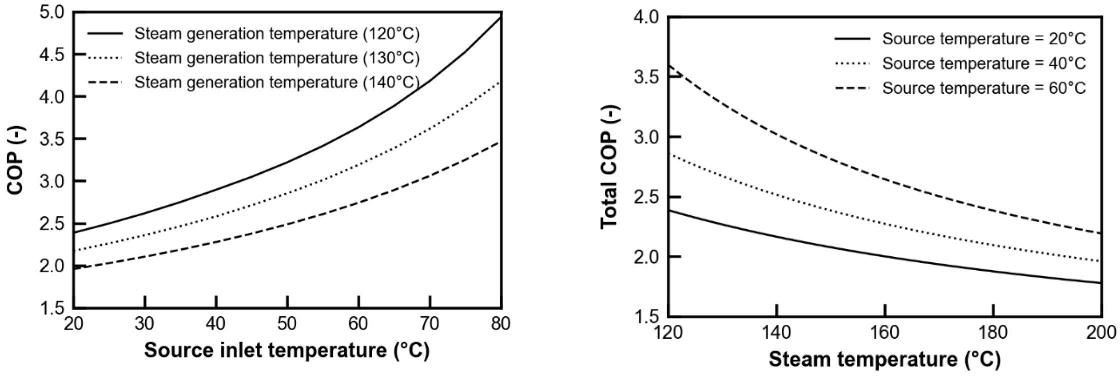


(a) (b)

Fig. 7. (a) Maximum COP of the SGHP system with varying source temperature, and (b) total system COP with MVR

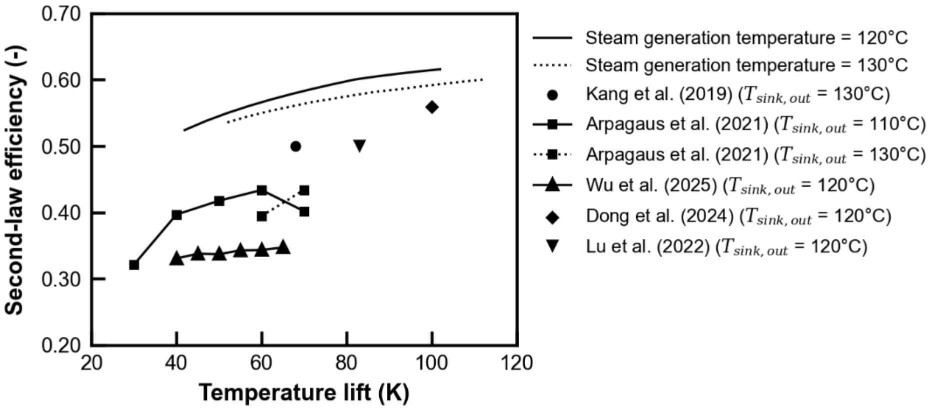


Fig. 8. Second-law efficiency comparison with previous studies

Fig. 8 compares the second-law efficiency of proposed system with previous studies, as direct COP comparison is difficult because the source and sink temperatures are not consistent across studies. The proposed system exhibits a much higher second-law efficiency compared with the single-stage compression SGHP with internal heat exchangers reported by Kang et al. and Arpagaus et al. [17-19]. It also achieves higher efficiency than cascade-type SGHP systems designed for large temperature lifts, particularly at temperature lifts above 80 K [5, 25]. Overall, the results indicate that the proposed SGHP system achieved superior efficiency across a wide range of temperature lifts compared with previously reported systems.

## 4. Conclusions

In this study, an SGHP system model featuring a three-stage compression and an internal heat exchanger was developed. The system performance was analysed through simulations to evaluate the effects of the number of compression stages on large temperature lift operation, as well as the impact of the implementation and configuration of the internal heat exchanger. The proposed system improved performance by optimizing the multi-compression cycle and internal heat exchanger arrangement, resulting in higher COP and second-law efficiency compared with previous studies, as verified through simulation. If the model is experimentally validated, it could be applied as SGHP system for large temperature difference applications. Furthermore, it may be combined with MVR to reach higher steam temperatures. Although the proposed system requires a large displacement volume in the bottom stage compressor relative to its heating capacity due to the low refrigerant density, it can still be applied to heating capacities of up to a few hundred kilowatts, even with a very low heat source temperature of around 20°C.

## Nomenclature

Roman symbol

| | |
|---|---|
| $A$ | heat transfer surface area, [m$^2$] |
| $C$ | heat capacity rate, [W/K] |
| $h$ | specific enthalpy, [J/kg/K] |
| $k$ | thermal conductivity, [W/m/K] |
| $K_v$ | valve flow coefficient |
| $L$ | plate thickness, [m] |
| $\dot{m}$ | mass flow rate, [kg/s] |
| $P$ | pressure, [Pa] |
| Q | heat transfer rate, [W] |
| $R$ | specific gas constant, [J/kg/K] |
| $R_f$ | fouling thermal resistance, [K/W] |
| $T$ | temperature, [K] |
| $U$ | overall heat transfer coefficient, [W/m$^2$/K] |
| $\dot{V}$ | volumetric flow rate, [m$^3$/s] |
| $\dot{W}$ | power, [W] |

Greek symbols

| | |
|---|---|
| $\alpha$ | heat transfer coefficient, [W/m$^2$/K] |
| $\Delta$ | difference |
| $\varepsilon$ | heat exchanger effectiveness |
| $\eta$ | efficiency |
| $\gamma$ | specific heat ratio |
| $\rho$ | density, [kg/m$^3$] |

## Acknowledgements

This work was supported by the Korea Institute of Energy Technology Evaluation and Planning (KETEP) grant funded by the Ministry of Trade, Industry & Energy (MOTIE, Korea) (No. 00236480).

## References

[1] Philibert, C., *Renewable energy for industry*. Paris: International Energy Agency; 2017.

[2] Arpagaus, C., Bless, F., Uhlmann, M., Schiffmann, J, Bertsch, S.S., 2018. High temperature heat pumps: Market overview, state of the art, research status, refrigerants, and application potentials. Energy 152, p. 985-1010.

[3] Bouckaert, S., Pales, A.F., McGlade, C., Remme, U., Wanner, B., Varro, L. et al. 2021, Net zero by 2050: A roadmap for the global energy sector.

[4] Mateu-Royo, C., Arpagaus, C., Mota-Babiloni, A., Navarro-Esbrí, J., Bertsch, S.S., 2021. Advanced high temperature heat pump configurations using low GWP refrigerants for industrial waste heat recovery: A comprehensive study. Energy Convers. Manag. 229, 113752.

[5] Lu, Z., Yao, Y., Liu, G., Ma, W., Gong, Y., 2022. Thermodynamic and Economic Analysis of a High Temperature Cascade Heat Pump System for Steam Generation. Processes 10, 9.

[6] Sulaiman, A.Y., Cotter, D.F., Le, K.X, Huang, M.J, Hewitt, N.J., 2022. Thermodynamic analysis of subcritical High-Temperature heat pump using low GWP Refrigerants: A theoretical evaluation. Energy Convers. Manag. 268, 116034.

[7] Ma, X., Du, Y., Zhao, T., Zhu, T., Lei, B., Wu, Y., 2024. A comprehensive review of compression high-temperature heat pump steam system: Status and trend. Int. J. Refrig. 164, p. 218-242.

[8] El Samad, T., Żabnieńska-Góra, A., Jouhara, H., Sayma, A.I., 2024. A review of compressors for high temperature heat pumps. Therm. Sci. Eng. Prog. 51, 102603.

[9] Bamigbetan, O., Eikevik, T.M, Nekså, P., Bantle, M., Schlemminger, C., 2018. Theoretical analysis of suitable fluids for high temperature heat pumps up to 125°C heat delivery. Int. J. Refrig. 92, p. 185-195.

[10] Jiang, J., Hu, B., Wang, R.Z., Liu, H., Zhang, Z., Li, H., 2021. Theoretical performance assessment of low-GWP refrigerant R1233zd (E) applied in high temperature heat pump system. Int. J. Refrig. 131, p. 897-908.

[11] Jiang, J., Hu, B., Wang, R.Z., Ge, T., Liu, H., Zhang, Z., Zhou, Y., 2023. Experiments of advanced centrifugal heat pump with supply temperature up to 100 °C using low-GWP refrigerant R1233zd(E). Energy 263, 126033.

[12] Klute, S., Budt, M., van Beek, M., Doetsch, C., 2024. Steam generating heat pumps – Overview, classification, economics, and basic modeling principles. Energy Convers. Manag. 299, 117882.
[13] Kosmadakis, G., Arpagaus, C., Neofytou, P., Bertsch, S., 2020. Techno-economic analysis of high-temperature heat pumps with low-global warming potential refrigerants for upgrading waste heat up to 150 °C. Energy Convers. Manag. 226, 113488.
[14] Adamson, K.M., Walmsley, T.G., Carson, J.K., Chen, Q., Schlosser, F., Kong, L., Cleland, D.J., 2022. High-temperature and transcritical heat pump cycles and advancements: A review. Renew. Sustain. Energy Rev. 167, 112798.
[15] Jiang, J., Hu, B., Wang, R.Z., Deng, N., Cao, F., Wang, C.C., 2022. A review and perspective on industry high-temperature heat pumps. Renew. Sustain. Energy Rev. 161, 112106.
[16] Ma, X., Du, Y., Lei, B., Wu, Y., 2024. Energy, exergy, economic, and environmental analysis of a high-temperature heat pump steam system. Int. J. Refrig. 160, p. 423-436.
[17] Arpagaus, C., Bless, F., Uhlmann, M., Büchel, E., Frei, S., Schiffmann, J., Bertsch, S., 2018. "High temperature heat pump using HFO and HCFO refrigerants-System design, simulation, and first experimental results," In: International Refrigeration and Air Conditioning Conference. West Lafayette, IN, USA, Paper 1875.
[18] Arpagaus, C., Bertsch, S.S., 2021. "Experimental comparison of HCFO and HFO R1224yd (Z), R1233zd (E), R1336mzz (Z), and HFC R245fa in a high temperature heat pump up to 150 °C supply temperature," In: International Refrigeration and Air Conditioning Conference. West Lafayette, IN, USA, Paper 2200.
[19] Kang, D.H., Na, S., Yoo, J.W., Lee, J.H., Kim, M.S., 2019. Experimental study on the performance of a steam generation heat pump with the internal heat exchanging effect. Int. J. Refrig. 108, p. 154-162.
[20] Wu, D., Wei, J., Hu, B., 2025. Theoretical analysis, experimental research and industrial verification of high temperature heat pump based on R1233zd (E). Energy 319, 135175.
[21] Peng, Z.R., Wang, G.B., Zhang, X.R., 2019. Thermodynamic analysis of novel heat pump cycles for drying process with large temperature lift. Int. J. Energy Res. 43, p. 3201-3222.
[22] Hamid, K., Sajjad, U., Ahrens, M.U., Ren, S., Ganesan, P., Tolstorebrov, I. et al. 2023. Potential evaluation of integrated high temperature heat pumps: A review of recent advances. Appl. Therm. Eng. 230, 120720.
[23] Liu, Y., Qu, S., Shen, S., Feng, Y., Sun, T., Wang, C., Xing, Z., 2025. Experimental investigation on the large temperature lift heat pump with an integrated two-stage independently variable frequency compressor. Energy 314, 134289.
[24] Shen, Y., Ma, Z., Fu, H., Ye, J., Sun, L., 2025. Thermodynamic modeling and analysis of cascade heat pump enhanced by vapor injection for steam production. Energy Sources, Part A: Recovery, Utilization, and Environmental Effects 47, p. 693-711.
[25] Dong, Y., Yan, H., Wang, R., 2024. Significant thermal upgrade via cascade high temperature heat pump with low GWP working fluids. Renew. Sustain. Energy Rev. 190, 114072.
[26] Ma, X., Du, Y., Wu, Y., Lei, B., Zhang, C., 2024. Performance evaluation and optimization guidance for steam generating heat pumps with significant temperature lift. Case Stud. Therm. Eng. 63, 105351.
[27] Ma, X., Du, Y., Li, B., Zhang, C., 2025. Enhanced thermal output from air-source cascade heat pumps configuration for steam generation. Case Stud. Therm. Eng. 75, 107112.
[28] Lemmon, E.W., Bell, I.H., Huber, M.L., McLinden, M.O., 2018. REFPROP 10.0, NIST Stand Reference Database 23.
[29] Lee, D., Kim, D., Park, S., Lim, J., Kim, Y., 2018. Evaporation heat transfer coefficient and pressure drop of R-1233zd(E) in a brazed plate heat exchanger. Appl. Therm. Eng. 130, p.1147-1155.
[30] Kwon, O.J., Shon, B., Kang, Y.T., 2019. Experimental investigation on condensation heat transfer and pressure drop of a low GWP refrigerant R-1233zd(E) in a plate heat exchanger. Int. J. Heat Mass Transf. 131, p. 1009-1021.